Asian Journal of Periodontics and Orthodontics
2024, Volume 4, Page No: 121-138
Copyright CC BY-NC-SA 4.0
Available online at: www.tsdp.net

ISSN: 3062-3499

Original Article

Finite Element Analysis of Trabecular Bone Response to Orthodontic Forces in Periodontal Breakdown

Mariana Ganea[1], Olivia Andreea Marcu[1]*, Andrei Nicolae Csep[2]*

[1]Department of Cariology, Endodontics and Oral Pathology, School of Dental Medicine, University of Medicine and Pharmacy Iuliu Hatieganu, Str. Motilor 33, 400001 Cluj-Napoca, Romania.
[2]Department of Orthodontics, School of Dental Medicine, University of Medicine and Pharmacy Iuliu Hatieganu, Cluj-Napoca, Str. Avram Iancu 31, 400083 Cluj-Napoca, Romania.

***E-mail** ✉ Anderinicocsep@mail.ru

Received: 01 August 2024; **Revised:** 11 November 2024; **Accepted:** 19 November 2024

ABSTRACT

This study used numerical simulations to evaluate how trabecular bone responds to orthodontic forces of 0.6, 1.2, and 2.4 N applied through five movement types—intrusion, extrusion, tipping, rotation, and translation—during progressive horizontal periodontal loss of 0–8 mm. Stress distribution, as well as ischemic and resorptive risks, were analyzed using the Tresca and Von Mises failure criteria. A total of 405 simulations were performed on 81 models derived from nine patients. Both criteria produced similar stress patterns qualitatively, while Tresca values were 1.09–1.21 times higher than Von Mises quantitatively. No qualitative differences were observed between the three force magnitudes, though a twofold increase was noted at 1.2 N and a fourfold increase at 2.4 N relative to 0.6 N. Among the movements, rotation and translation generated the greatest stresses, followed by tipping, particularly in cases of reduced periodontium where ischemic and resorptive risks were more pronounced. Forces of 1.2 N appeared safe in intact periodontium, but for reduced periodontium, only extrusion and intrusion could tolerate this level without elevated risk. Loads exceeding 0.6 N for the other movements increased ischemic and resorptive potential. In intact periodontium, stress was distributed throughout the trabecular structure, while in reduced periodontium, stress concentrated near the cervical third of the alveolar socket once bone loss reached 4 mm, indicating a clear shift in stress distribution.

Keywords: Trabecular bone, Failure criteria, Periodontal breakdown, Light orthodontic force, Finite element analysis, Orthodontic movements

How to Cite This Article: Ganea M, Marcu OA, Csep AN. Finite Element Analysis of Trabecular Bone Response to Orthodontic Forces in Periodontal Breakdown. Asian J Periodont Orthodont. 2024;4:121-38. https://doi.org/10.51847/DVdnjkDpYE

Introduction

The mandibular bone primarily functions as a structural support and protective framework, and its internal microarchitecture is crucial during orthodontic interventions [1–3]. When bone integrity is preserved, load transfer—through stress absorption and dispersion—is optimal; however, progressive periodontal breakdown alters bone height and consequently modifies its biomechanical behavior [1–3]. Despite its clinical importance, data concerning the biomechanics of alveolar bone loss remain scarce [1, 2].

Previous finite element analyses (FEA) have extensively focused on implant–bone interactions [4–12], with only a limited number exploring tooth–bone mechanics [13–15]. These investigations generally evaluated stress distributions in intact periodontium under one or two loading conditions, often yielding inconsistent or clinically incongruent findings [4–16]. Moreover, there remains a notable absence of studies that separately analyze the cortical and trabecular bone components—an essential distinction, particularly in cases of partial bone resorption.

To maintain remaining bone integrity during orthodontic therapy, it is vital to understand how orthodontic forces are distributed, where stress concentrations occur, and how these relate to disease progression, since periodontal disorders affect both

© 2024 Asian Journal of Periodontics and Orthodontics

young and elderly populations [2–4, 17]. From a biomechanical perspective, the bone's internal lattice enables elastic deformation while maintaining structural efficiency with minimal material volume [1, 3, 4, 17–19]. The cortical layer, being denser and more mineralized, provides rigidity and protection [1, 3, 4, 17, 18], while the trabecular core—housing marrow, vasculature, and neural elements—supports regenerative and nutritive functions [1, 17, 18, 20].

As bone resorption progresses, the biomechanical response shifts. Applying the same orthodontic force suitable for intact bone can lead to ischemic and resorptive effects, potentially accelerating tissue degradation and negatively influencing treatment outcomes [1, 17, 20]. The finite element method remains the sole viable approach for evaluating stress distributions in individual tissue types under diverse mechanical scenarios [2, 4–6, 11, 16, 19, 21–24]. While FEA has gained wide acceptance in dentistry over the past two decades, numerous studies have presented contradictory or clinically inconsistent results [1, 2, 17, 23]. In contrast, within engineering, the same computational framework has demonstrated high accuracy and reliability [1, 2, 17, 20, 22, 23]. These discrepancies stem from inadequate use of failure criteria, unrealistic boundary conditions, and anatomically imprecise 3D geometries [1, 17, 22, 23].

Earlier dental FEA models [4–15, 24] often lacked methodological rigor—applying failure criteria without justification, using simplified geometries, and neglecting key physiological constants, such as the maximum hydrostatic pressure (MHP) of 16–22 kPa (≈80% of systolic pressure) [23]. Exceeding this threshold may provoke ischemia and bone resorption. Only three early studies examined bone–tooth stress within intact periodontium—at 0.35–0.5 N tipping [13, 14], 10 N intrusion, and 3 N tipping/translation [15]—employing Von Mises and maximum principal stress criteria, but without reference to MHP or material behavior, producing variable, clinically inconsistent outcomes.

However, prior biomechanical research from our group demonstrated that accurate simulations can be achieved when FEA guidelines are rigorously followed [1, 17]. Suitable criteria include Von Mises (VM) for homogeneous and Tresca (T) for non-homogeneous, ductile-like dental tissues, provided anatomically precise 3D reconstructions (from CBCT scans with voxel sizes ≤0.075 mm) are utilized [1, 2, 17, 20, 22, 23]. The assumptions of linear elasticity, isotropy, and non-homogeneity remain valid for orthodontic forces up to 2.4 N (240 gf) [1, 17]. Nevertheless, numerical outcomes must always be interpreted alongside clinical and physiological data, as FEA cannot fully replicate in vivo conditions [24].

When applied forces exceed structural tolerance, both trabecular and cortical bone exhibit microdamage, including microcracks and diffuse microfractures, which typically heal rapidly [25]. These defects often arise near resorption zones, altering local biomechanics [25]. Age-related changes also affect stress response—younger bone being more ductile and tension-sensitive, while older bone becomes brittle, showing greater susceptibility to compressive microfractures [25]. Consequently, aged trabecular bone experiences mixed brittle–ductile deformation patterns when exposed to shear stresses [25].

The brittle material typically lacks the ability to deform and tends to fracture or develop cracks when subjected to external forces [1, 2, 17].

Conversely, ductile substances undergo elastic deformation under loading and return to their initial shape once the force is removed [1, 2, 17].

Bone exhibits a mixed mechanical response, behaving in a ductile-like manner yet showing certain brittle flow characteristics that vary with age [1, 17].

From a microstructural standpoint, bone represents a heterogeneous, anisotropic continuum.

It is essential to note that bone biomechanics are complex and multifactorial, being influenced by both its structural composition and intrinsic material properties [26].

When orthodontic forces are exerted, the periodontal ligament (PDL) absorbs and disperses most of the resulting stress, while the remaining portion is transferred to the bone, causing reversible elastic deformation [1, 17, 20, 22].

However, in cases of periodontal degradation, as the PDL diminishes, stress concentration at the bone interface increases—particularly in trabecular bone, which is more prone to ischemic damage and subsequent resorption due to its vascular nature [1, 17, 20].

In biomechanical physics, interactions between materials with differing elastic moduli (**(Table 1)**; higher modulus = less deformation [6, 21]) lead to maximum stress accumulation at contact regions, such as the cervical third of bone [1, 17, 22].

Table 1. Elastic properties of materials.

Substance	Elastic Modulus, E (GPa)	Poisson's Ratio, υ	References
Enamel	80	0.33	[1, 2, 17, 20, 22, 23]
Dentin/Cementum	18.6	0.31	[1, 2, 17, 20, 22, 23]

Pulp	0.0021	0.45	[1, 2, 17, 20, 22, 23]
Periodontal Ligament	0.0667	0.49	[1, 2, 17, 20, 22, 23]
Cortical Bone	14.5	0.323	[1, 2, 17, 20, 22, 23]
Trabecular Bone	1.37	0.3	[1, 2, 17, 20, 22, 23]
Stainless Steel	190	0.265	[1, 2, 17, 20, 22, 23]

Finite element analyses (FEA) of bone–implant systems commonly use von Mises (VM) criteria in healthy periodontium models, identifying stress concentration in the cortical cervical third of the implant site and broader stress dispersion in the trabecular region due to its higher ductility [4–11, 15]. Shear stress has been associated with implant socket resorption [5].

To minimize ischemic and resorptive damage, forces should remain below the maximum hydrostatic pressure (MHP), particularly within the PDL and neurovascular regions.

Despite being less deformable and less vascularized, trabecular bone can endure higher loads without structural failure.

Orthodontic movement results from circulatory alterations within both the PDL and trabecular bone, prompting bone remodeling [19, 27–29].

When bone loss occurs or circulatory disturbances persist, ischemia contributes to further resorption.

Clinically, the safe orthodontic force for a healthy periodontium is estimated at up to 1.5 N (150 gf) [1, 2, 17, 30], though consensus is lacking, and no precise data exist for compromised periodontal conditions.

Another clinical complication during orthodontic therapy related to ischemic and resorptive effects is external orthodontic root resorption [31–40].

Both internal [41] and external [2] root resorption represent unpredictable adverse effects [33–35], involving dentin and cementum in both the root (apical/cervical) [2, 41, 42] and crown regions [33, 36, 37].

The biomechanical mechanism remains not fully clarified [43–47], but microscopic lacunae can develop within 10–35 days under continuous force application [33, 37–39].

The recommended safe force for intact periodontium ranges between 0.5–1 N [2, 41], though other reports extend the range from 0.28 to 3.31 N [19, 24, 48–52], leaving the matter under debate.

To date, no investigations have explored root resorption in reduced periodontium, aside from our previous study [2, 41].

Additional contributing factors include age, ethnicity, systemic conditions (e.g., osteoporosis, genetic syndromes), trauma history, or prior endodontic treatment [31, 32, 40, 42, 49, 53–59].

Before exploring trabecular bone at the cellular level, it is necessary to establish a macro-level understanding of stress distribution across the entire structure.

We observed that no prior studies have evaluated stress distribution in trabecular bone during periodontal degradation, nor assessed how bone loss modifies loading patterns or whether orthodontic force should be adjusted accordingly—making our study the first to address this topic.

Hence, our objectives were:

a. to biomechanically evaluate trabecular bone under mild orthodontic forces and five movement types during horizontal periodontal bone loss;
b. to analyze stress distribution alterations within trabecular bone caused by bone loss; and
c. to determine ischemic and resorptive risks by comparing findings with MHP limits, previous FEA data, and clinical evidence.

Materials and Methods

This work forms part of an extended sequential investigation (clinical approval no. 158/02.04.2018) designed to numerically examine how dental tissues respond biomechanically to orthodontic forces and movements occurring during periodontal deterioration.

Patient selection.

In this phase, emphasis was placed on trabecular bone evaluation, based on 81 three-dimensional (3D) digital models of the second mandibular premolar, resulting in 405 individual finite element simulations.

The dataset included nine participants (4 men and 5 women; mean age = 29.81 ± 1.45 years), consistent with our prior publications [1, 2, 17, 20, 22, 23].

Compared with previous finite element analysis (FEA) works—each usually limited to a single model or patient [4–15, 21, 27, 28]—this study involved a nine-fold larger sample size, allowing for greater variability and robustness.

FEA models commonly rely on one individual because even small changes in input parameters can generate distinct simulation outcomes.

Eligibility criteria.

Inclusion parameters required a complete mandibular dentition, absence of tooth crowding or rotation, no prior restorations, endodontic therapy, or crowns, non-inflamed periodontal tissues, minimal bone loss, a

clinical indication for orthodontic treatment, and satisfactory oral hygiene.

Exclusion parameters included unusual root morphology (bifurcations, pronounced curvature), atypical crown shape, deciduous teeth, root or bone surface irregularities (external resorption or visible osseous defects), internal root resorption, bone loss greater than 2–3 mm, or poor periodontal health at the time of enrollment.

The region of interest comprised mandibular premolars and molars, imaged with cone-beam computed tomography (CBCT) using a ProMax 3DS scanner (Planmeca, Helsinki, Finland) at 0.075 mm voxel resolution.

The lower jaw was selected because earlier FEA literature mainly explored incisor and molar regions, with limited attention given to this anatomical zone.

Model development.

The DICOM image sets, representing various grayscale intensities, were processed in Amira 5.4.0 (Visage Imaging Inc., Andover, MA, USA).

Because of the intricate micro-architecture of dental structures, a single experienced operator manually reconstructed each model to maintain accuracy and reduce interpretation bias.

Individual components—enamel, dentin, pulp, neurovascular bundle (NVB), periodontal ligament (PDL), cortical bone, and trabecular bone—were identified and digitally segmented **(Figure 1)**.

The cementum layer was not modeled separately; due to its similar physical behavior to dentin **(Table 1)**, it was merged with the dentin structure.

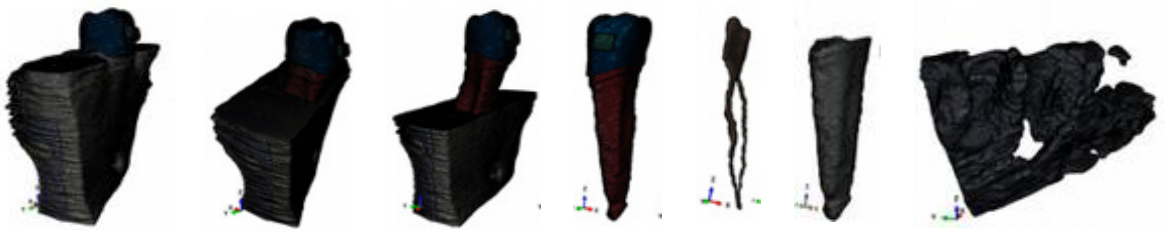
The PDL thickness ranged between 0.15 mm and 0.225 mm and enclosed the NVB.

All tissues were assembled into 3D composite models of the second mandibular premolar, each featuring different degrees of cervical bone loss.

Adjacent teeth were omitted, and their sockets were filled with trabecular and cortical bone material.

A metal bracket base was digitally positioned on the buccal crown surface to avoid interference from the bracket slot.

Missing PDL and bone were reconstructed manually to match anatomical conditions, yielding nine baseline models representing intact periodontal support.



a) b) c) d) e) f) g)

Figure 1. Mesh configurations: a) premolar with intact periodontium; b) 4 mm bone loss; c) 8 mm bone loss; d) premolar tooth; e) pulp; f) healthy PDL; g) trabecular bone within intact periodontium.

Each intact model was sequentially modified by reducing the alveolar crest 1 mm at a time, from 0 mm to 8 mm, generating nine bone-loss stages per model and totaling 81 model variants.

The intact-periodontium versions contained approximately 5.06–6.05 million C3D4 tetrahedral elements, 0.97–1.07 million nodes, and a global mesh size of 0.08–0.116 mm **(Figures 1 and 2)**.



a) b) c) d) e) f) g)

Figure 2. Boundary configurations: a) extrusion vectors; b) element warnings in trabecular bone; c) trabecular cone under intact periodontium; d) intrusion; e) tipping; f) rotation; g) translation.

The manually generated models displayed only a small number of element warnings and no mesh errors **(Figure 2)**.

Such alerts corresponded to minor surface inconsistencies in non-critical regions, whereas stress zones remained continuous and stable.

All models successfully met the software's internal validation checks.

The model with the most detailed mesh exhibited 264 warnings (0.0043% of 6.05 million elements), of which 70 (0.0041% of 1,699,730 elements) originated from the trabecular bone **(Figure 2)**.

Finite element analysis (FEA).

The simulations were executed using Abaqus 6.13-1 (Dassault Systèmes Simulia Corp., Maastricht, Netherlands).

Five standard orthodontic tooth movements were tested—intrusion, extrusion, translation, rotation, and tipping—each under three force levels: 0.6 N (≈60 gf), 1.2 N (≈120 gf), and 2.4 N (≈240 gf).

Forces were applied to the bracket region, and the base of each model was fixed (encastered) with ideal bonding conditions among components.

These magnitudes were chosen because they are considered clinically safe for a healthy periodontium.

Assumptions of linear elasticity, isotropy, and homogeneity/non-homogeneity were maintained, following methodologies used in previous FEA literature [4–15, 21, 27, 28], and validated by our earlier data showing these assumptions remain valid up to 2.4 N [1, 17].

The Von Mises (for total stress in homogeneous materials) and Tresca (for shear stress in non-homogeneous materials) criteria were applied to evaluate failure behavior.

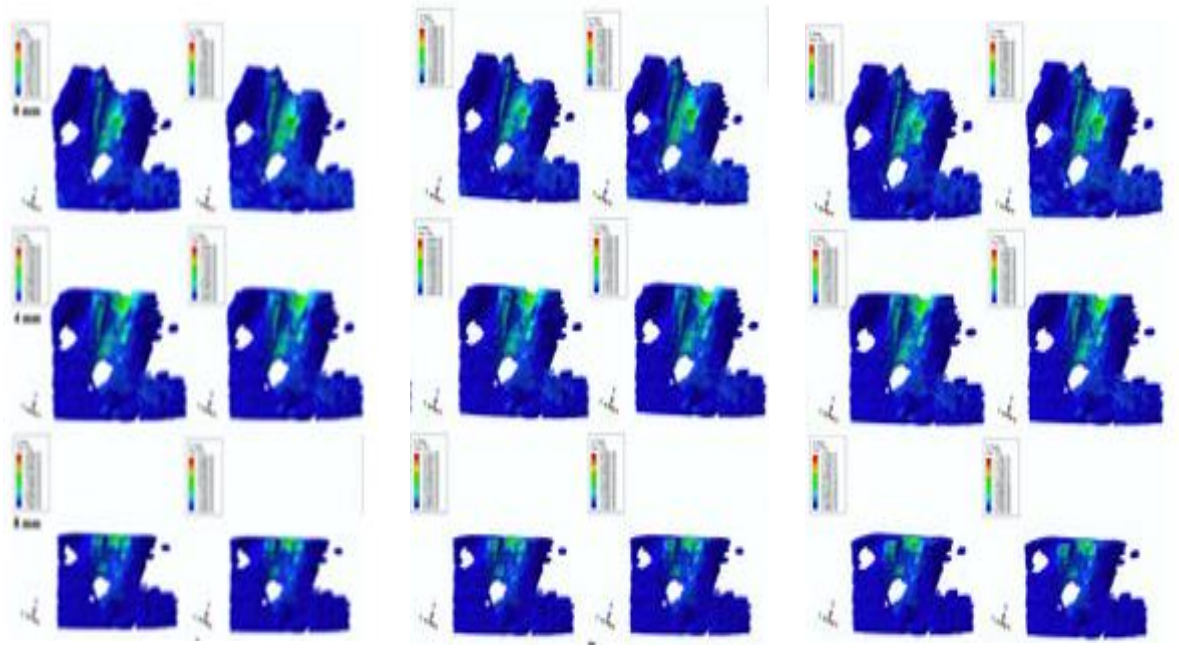
Stress intensity was represented with color maps (red-orange = high, yellow-green = medium, blue = low), along with quantitative results for each of the 81 scenarios.

Stress distribution was assessed in the cervical, middle, and apical thirds of the alveolar socket.

Values were compared with the maximum hydrostatic pressure (MHP) threshold of 16–22 kPa, previous FEA findings, and clinical references to determine accuracy and assess ischemic or resorptive potential.

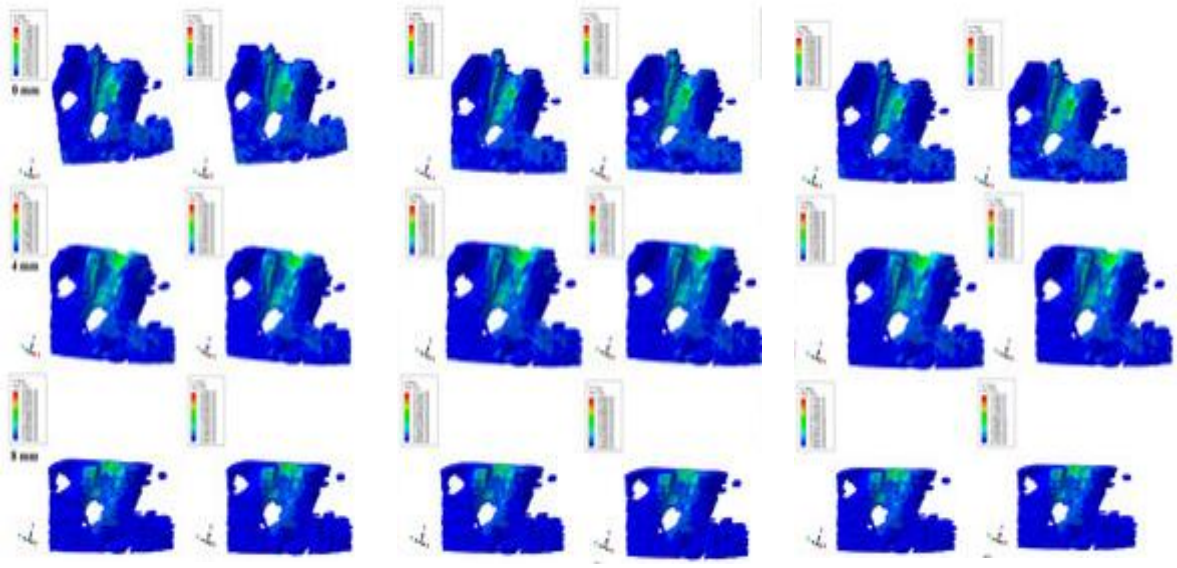
Results and Discussion

In this computational study, a total of 405 simulation trials were conducted using eighty-one three-dimensional mandibular models **(Figures 3–7 and Table 2)**. The findings include both descriptive (qualitative) and numerical (quantitative) outcomes.



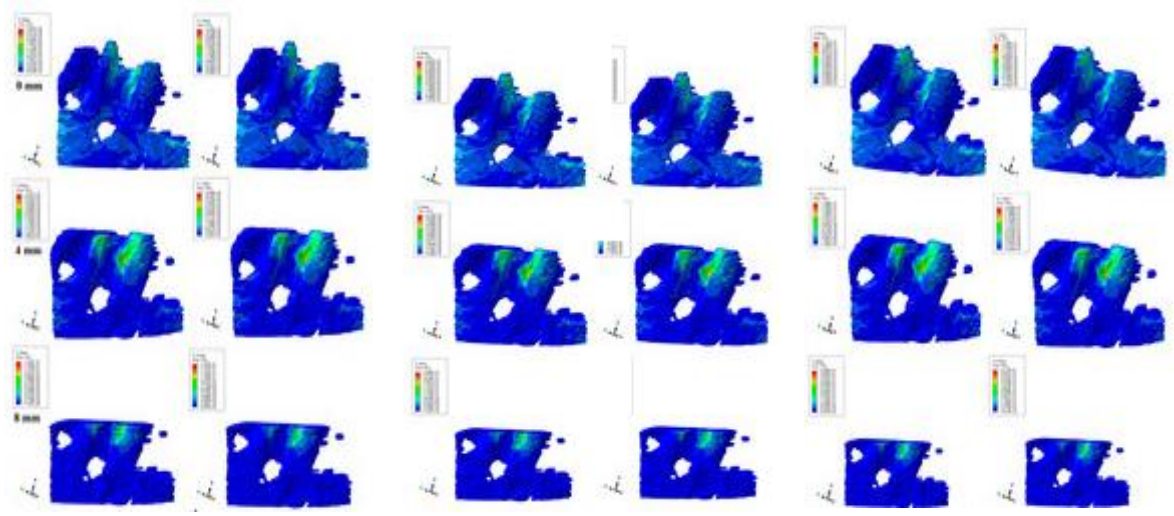
a) b) c)

Figure 3. Stress comparison based on Von Mises and Tresca criteria for intact bone and for 4 mm and 8 mm periodontal loss during intrusive loading of 0.6 (a), 1.2 (b), and 2.4 N (c).



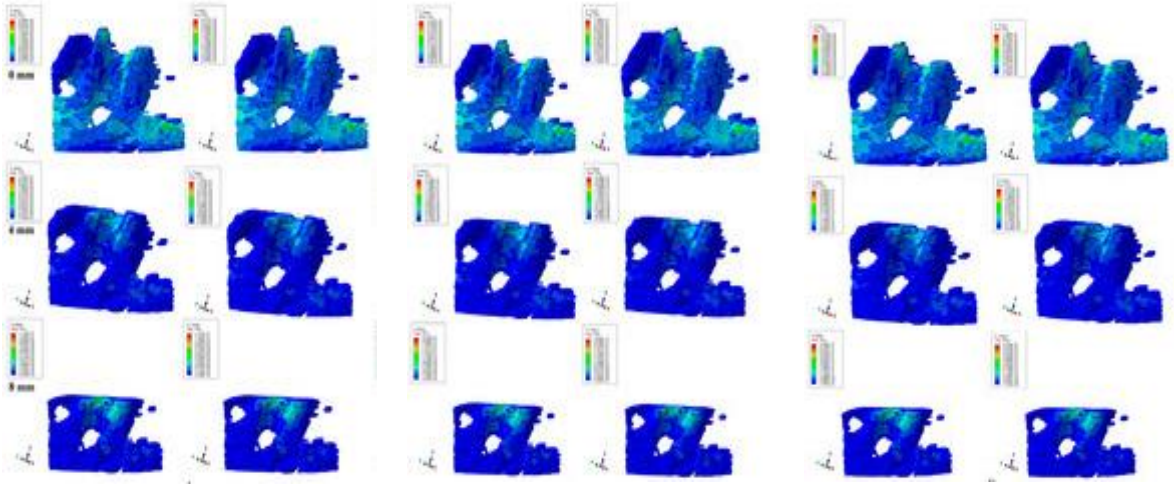
a) b) c)

Figure 4. Corresponding comparison for extrusive loading under the same conditions.



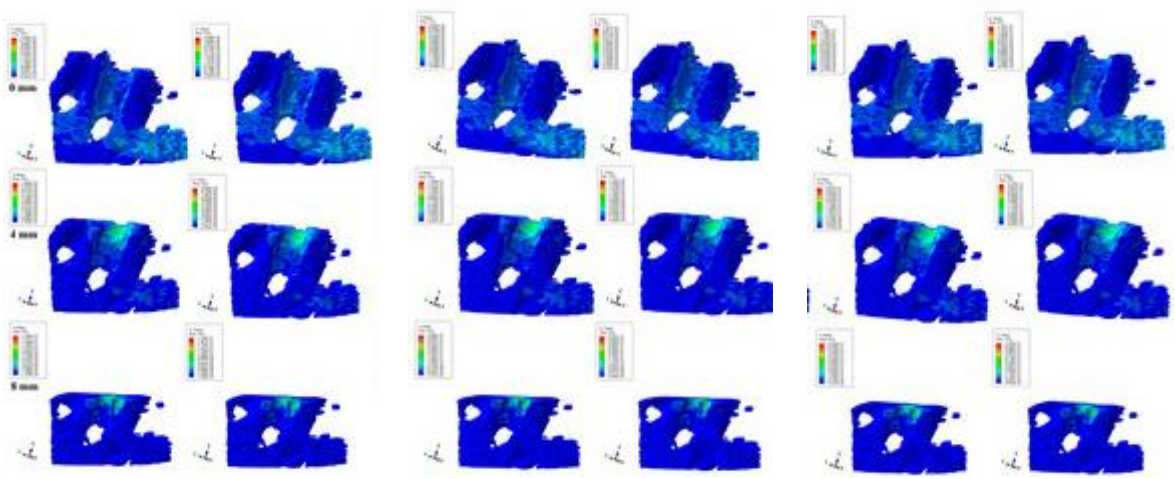
a) b) c)

Figure 5. Stress mapping for translational movement at identical load levels.



a) b) c)

Figure 6. Visualization of rotational movement stresses.



a) b) c)

Figure 7. Stress distribution for tipping motion under forces of 0.6, 1.2, and 2.4 N.

Table 2. Mean peak stress values (kPa) produced by the three orthodontic load magnitudes.
a—apical region, m—middle region, c—cervical region.

Movement Type	Stress Criterion	Region	Resorption (mm) 0	1	2	3	4	5	6	7	8
Intrusion	Tresca	Apical (a)	4.13	4.20	4.27	4.34	4.42	5.16	5.90	6.64	7.38
0.6 N/60 gf		Middle (m)	8.31	8.97	9.64	10.30	10.97	12.86	14.75	16.64	18.43
		Cervical (c)	11.07	13.23	15.39	17.55	19.72	23.07	26.43	29.78	33.14
	von Mises (VM)	Apical (a)	2.97	3.19	3.41	3.64	3.86	4.51	5.15	5.80	6.44
		Middle (m)	7.28	7.87	8.44	9.02	9.61	11.22	12.84	14.46	16.08
		Cervical (c)	10.18	11.95	13.72	15.49	17.26	20.17	23.09	26.00	28.92
Intrusion	Tresca	Apical (a)	8.26	8.40	8.54	8.68	8.83	10.32	11.80	13.28	14.77
1.2 N/120 gf		Middle (m)	16.63	17.94	19.28	20.60	21.95	25.72	29.50	33.28	36.86
		Cervical (c)	22.14	26.46	30.78	35.10	39.45	46.14	52.86	59.56	66.28
	von Mises (VM)	Apical (a)	5.94	6.38	6.83	7.27	7.73	9.01	10.30	11.59	12.89
		Middle (m)	14.56	15.73	16.88	18.04	19.21	22.44	25.68	28.92	32.17
		Cervical (c)	20.36	23.90	27.44	30.98	34.52	40.34	46.18	52.00	57.85
Intrusion	Tresca	Apical (a)	16.52	16.80	17.08	17.36	17.66	20.64	23.60	26.56	29.53
2.4 N/240 gf		Middle (m)	33.25	35.88	38.56	41.20	43.89	51.44	59.00	66.56	73.72
		Cervical (c)	44.29	52.92	61.56	70.20	78.89	92.28	105.72	119.12	132.57
	von Mises (VM)	Apical (a)	11.88	12.77	13.66	14.55	15.46	18.02	20.60	23.18	25.77

		Middle (m)	29.12	31.46	33.76	36.08	38.43	44.88	51.36	57.84	64.34
		Cervical (c)	40.73	47.80	54.88	61.96	69.05	80.68	92.36	104.00	115.69
Extrusion	Tresca	Apical (a)	4.13	4.20	4.27	4.34	4.42	5.16	5.90	6.64	7.38
0.6 N/60 gf		Middle (m)	8.31	8.97	9.64	10.30	10.97	12.86	14.75	16.64	18.43
		Cervical (c)	11.07	13.23	15.39	17.55	19.72	23.07	26.43	29.78	33.14
	von Mises (VM)	Apical (a)	2.97	3.19	3.41	3.64	3.86	4.51	5.15	5.80	6.44
		Middle (m)	7.28	7.87	8.44	9.02	9.61	11.22	12.84	14.46	16.08
		Cervical (c)	10.18	11.95	13.72	15.49	17.26	20.17	23.09	26.00	28.92
Extrusion	Tresca	Apical (a)	8.26	8.40	8.54	8.68	8.83	10.32	11.80	13.28	14.77
1.2 N/120 gf		Middle (m)	16.63	17.94	19.28	20.60	21.95	25.72	29.50	33.28	36.86
		Cervical (c)	22.14	26.46	30.78	35.10	39.45	46.14	52.86	59.56	66.28
	von Mises (VM)	Apical (a)	5.94	6.38	6.83	7.27	7.73	9.01	10.30	11.59	12.89
		Middle (m)	14.56	15.73	16.88	18.04	19.21	22.44	25.68	28.92	32.17
		Cervical (c)	20.36	23.90	27.44	30.98	34.52	40.34	46.18	52.00	57.85
Extrusion	Tresca	Apical (a)	16.52	16.80	17.08	17.36	17.66	20.64	23.60	26.56	29.53
2.4 N/240 gf		Middle (m)	33.25	35.88	38.56	41.20	43.89	51.44	59.00	66.56	73.72
		Cervical (c)	44.29	52.92	61.56	70.20	78.89	92.28	105.72	119.12	132.57
	von Mises (VM)	Apical (a)	11.88	12.77	13.66	14.55	15.46	18.02	20.60	23.18	25.77
		Middle (m)	29.12	31.46	33.76	36.08	38.43	44.88	51.36	57.84	64.34
		Cervical (c)	40.73	47.80	54.88	61.96	69.05	80.68	92.36	104.00	115.69
Translation	Tresca	Apical (a)	8.06	8.26	8.46	8.66	8.87	9.88	10.90	11.92	12.94
0.6 N/60 gf		Middle (m)	17.08	19.14	21.20	23.26	25.32	35.08	44.85	54.61	64.38
		Cervical (c)	22.74	28.65	34.56	40.47	46.38	63.75	81.12	98.49	115.87
	von Mises (VM)	Apical (a)	7.05	7.24	7.43	7.62	7.81	8.68	9.55	10.42	11.30
		Middle (m)	14.88	16.91	18.95	20.98	23.02	31.31	39.60	47.89	56.18
		Cervical (c)	19.81	25.39	30.98	36.56	42.15	56.89	71.63	86.37	101.12
Translation	Tresca	Apical (a)	16.12	16.52	16.92	17.32	17.75	19.76	21.80	23.84	25.89
1.2 N/120 gf		Middle (m)	34.17	38.28	42.40	46.52	50.64	70.16	89.70	109.22	128.76
		Cervical (c)	45.48	57.30	69.12	80.94	92.75	127.50	162.24	196.98	231.74
	von Mises (VM)	Apical (a)	14.10	14.48	14.86	15.24	15.61	17.36	19.10	20.84	22.60

		Middle (m)	29.76	33.82	37.90	41.96	46.04	62.62	79.20	95.78	112.36
		Cervical (c)	39.63	50.78	61.96	73.12	84.31	113.78	143.26	172.74	202.25
Translation	Tresca	Apical (a)	32.23	33.04	33.84	34.64	35.50	39.52	43.60	47.68	51.77
2.4 N/240 gf		Middle (m)	68.34	76.56	84.80	93.04	101.28	140.32	179.40	218.44	257.53
		Cervical (c)	90.97	114.60	138.24	161.88	185.50	255.00	324.48	393.96	463.48
	von Mises (VM)	Apical (a)	28.19	28.96	29.72	30.48	31.23	34.72	38.20	41.68	45.21
		Middle (m)	59.53	67.64	75.80	83.92	92.08	125.24	158.40	191.56	224.72
		Cervical (c)	79.25	101.56	123.92	146.24	168.62	227.56	286.52	345.48	404.50
Rotation	Tresca	Apical (a)	11.56	13.78	16.00	18.22	20.45	20.87	21.30	21.72	22.15
0.6 N/60 gf		Middle (m)	22.86	24.79	26.72	28.65	30.59	39.39	48.20	57.01	65.82
		Cervical (c)	22.86	37.47	52.00	66.71	81.33	91.12	100.91	110.70	120.50
	von Mises (VM)	Apical (a)	10.51	12.34	14.17	16.00	17.84	18.18	18.52	18.86	19.21
		Middle (m)	20.76	22.23	23.70	25.17	26.65	34.26	41.88	49.50	57.12
		Cervical (c)	20.76	33.27	45.78	58.29	70.81	79.24	87.67	96.10	104.53
Rotation	Tresca	Apical (a)	23.13	27.56	32.00	36.44	40.91	41.74	42.60	43.44	44.29
1.2 N/120 gf		Middle (m)	45.71	49.58	53.44	57.30	61.19	78.78	96.40	114.02	131.64
		Cervical (c)	45.71	74.94	104.00	133.42	162.65	182.24	201.82	221.40	240.99
	von Mises (VM)	Apical (a)	21.01	24.68	28.34	32.00	35.69	36.36	37.04	37.72	38.42
		Middle (m)	41.52	44.46	47.40	50.34	53.30	68.52	83.76	99.00	114.24
		Cervical (c)	41.52	66.54	91.56	116.58	141.62	158.48	175.34	192.20	209.06
Rotation	Tresca	Apical (a)	46.26	55.12	64.00	72.88	81.81	83.48	85.20	86.88	88.58
2.4 N/240 gf		Middle (m)	91.42	99.16	106.88	114.60	122.37	157.56	192.80	228.04	263.28
		Cervical (c)	91.42	149.88	208.00	266.84	325.31	364.48	403.64	442.80	481.98
	von Mises (VM)	Apical (a)	42.02	49.36	56.68	64.00	71.37	72.72	74.08	75.44	76.84
		Middle (m)	83.05	88.92	94.80	100.68	106.59	137.04	167.52	198.00	228.48
		Cervical (c)	83.05	133.08	183.12	233.16	283.24	316.96	350.68	384.40	418.12
Tipping	Tresca	Apical (a)	6.20	6.54	6.88	7.22	7.57	9.39	11.21	13.03	14.86
0.6 N/60 gf		Middle (m)	15.15	16.92	18.70	20.48	22.26	31.45	40.65	49.84	59.04

		Cervical (c)	15.15	22.44	29.73	37.02	44.31	59.05	73.79	88.53	103.28
	von Mises (VM)	Apical (a)	5.95	6.11	6.27	6.43	6.60	8.19	9.79	11.38	12.98
		Middle (m)	14.54	15.75	16.96	18.17	19.39	2.44	35.50	43.56	51.62
		Cervical (c)	14.54	20.54	26.55	32.56	38.57	51.48	64.40	77.31	90.23
Tipping	Tresca	Apical (a)	12.40	13.08	13.76	14.44	15.14	18.78	22.42	26.06	29.71
1.2 N/120 gf		Middle (m)	30.31	33.84	37.40	40.96	44.52	62.90	81.30	99.68	118.09
		Cervical (c)	30.31	44.88	59.46	74.04	88.61	118.10	147.58	177.06	206.56
	von Mises (VM)	Apical (a)	11.90	12.22	12.54	12.86	13.20	16.38	19.58	22.76	25.96
		Middle (m)	29.08	31.50	33.92	36.34	38.77	4.88	71.00	87.12	103.24
		Cervical (c)	29.08	41.08	53.10	65.12	77.13	102.96	128.80	154.62	180.46
Tipping	Tresca	Apical (a)	24.80	26.16	27.52	28.88	30.29	37.56	44.84	52.12	59.42
2.4 N/240 gf		Middle (m)	60.62	67.68	74.80	81.92	89.05	125.80	162.60	199.36	236.17
		Cervical (c)	60.62	89.76	118.92	148.08	177.23	236.20	295.16	354.12	413.11
	von Mises (VM)	Apical (a)	23.80	24.44	25.08	25.72	26.39	32.76	39.16	45.52	51.92
		Middle (m)	58.17	63.00	67.84	72.68	77.55	9.76	142.00	174.24	206.47
		Cervical (c)	58.17	82.16	106.20	130.24	154.27	205.92	257.60	309.24	360.93

From a numerical standpoint **(Table 2)**, both stress-evaluation methods showed that rotation and translation generated the greatest stresses, followed by tipping, whereas intrusion and extrusion resulted in the lowest levels. Hence, rotational and translational forces appeared to place the greatest mechanical demand on the trabecular bone.

When evaluating the intact periodontium, the application of 0.6 N forces yielded stress values that remained under the maximum hydrostatic pressure (MHP) threshold. A 1.2 N load proved acceptable for intrusion, extrusion, and tipping, though rotation and translation slightly exceeded the MHP at the middle and cervical thirds. In contrast, 2.4 N was within the safe range only for intrusive, extrusive, and tipping forces.

In models representing reduced periodontal support, 0.6 N produced stress values beneath the MHP for intrusion and extrusion even with 8 mm of bone loss, while for other movements, this safety held only up to 4 mm. Between 4 and 8 mm, stresses rose beyond the MHP—up to threefold in the middle third (for rotation at 8 mm loss) and sixfold in the cervical third (for rotation at 8 mm)—indicating significant ischemic and resorptive potential. A 1.2 N load remained relatively safe for intrusion and extrusion even at 8 mm loss, though stress at the cervical third doubled or tripled. However, rotation, translation, and tipping at the same load surpassed MHP soon after minor bone loss, implying heightened tissue risk. A 2.4 N force markedly exceeded MHP across all movements, suggesting considerable danger of ischemic and resorptive effects **(Table 2)**.

When comparing the two failure models, Tresca (T) generated slightly higher stress than Von Mises (VM) — approximately 1.09–1.21× greater in intact tissues and 1.13–1.16× in reduced ones. These differences align with the 1.15–1.30× range reported in previous studies. Both indicators exhibited a consistent rise in stress throughout the progression of periodontal deterioration, corresponding to known biomechanical trends. Importantly, all stress values remained below the established trabecular bone strength limits (compressive modulus 0.155 GPa, compressive strength 6 MPa [4–12]).

From a qualitative viewpoint, the two models produced nearly identical spatial stress distributions across all types of movement and degrees of bone loss, matching expected clinical behavior. Between the 0.6, 1.2, and 2.4 N forces, only the magnitude of stress varied — doubling at 1.2 N and quadrupling at 2.4 N relative to 0.6 N — while the areas affected stayed consistent. As periodontal breakdown advanced (notably after 4 mm of loss), stress became increasingly concentrated near the remaining alveolar socket, despite greater overall stress values.

For intrusive and extrusive movements **(Figures 3 and 4)**, the qualitative and quantitative findings were essentially parallel at every load and bone-loss level. Under intact conditions, stress visualization displayed mainly green coloration, indicating moderate stress and minimal ischemic risk, predominantly localized in the cervical and middle thirds around the alveolar socket (on lingual and proximal surfaces aligned with the force vector). As bone and ligament degradation progressed, the regions of peak stress shifted toward the cervical third (lingual, mesial, and distal areas) of the residual socket—especially visible beyond 4 mm loss—with yellow-green hues marking a greater ischemic tendency than in the healthy model.

Translational movement **(Figure 5)** demonstrated almost identical color-coded patterns for both failure models. In the intact periodontium, stress representation (mainly green tones, indicating moderate ischemic potential) extended over the entire alveolar socket, predominantly on the proximal side, consistent with the direction of applied force. Once 4 mm of bone loss occurred, red–orange areas (signifying elevated ischemic risk) emerged at the mesial and distal cervical thirds of the alveolar socket. Although translational movement in healthy tissues produced only mild stress (green), its distribution was wider (blue–green hues) across the trabecular bone. As the breakdown advanced—particularly beyond 4 mm—stress became increasingly localized near the socket margins, mainly within the cervical third, and with more intense yellow–green to red–orange zones.

Rotational movement **(Figure 6)** produced comparable stress patterns under both analyzed conditions. For the intact periodontium, this motion generated the broadest stress spread among all five movements, extending beyond the alveolar socket (lingual, mesial, and distal regions) into nearly the entire trabecular framework, while still appearing primarily in green tones on the color scale. When bone resorption progressed, stress became concentrated and intensified (yellow–green) surrounding the remaining cervical socket wall, a pattern already evident after 4 mm of tissue loss.

Tipping movement **(Figure 7)** displayed, in the healthy model, stress of blue–green intensity distributed throughout the trabecular matrix, with concentrations observed in the middle and apical thirds of the alveolar socket (mesial, distal, and lingual zones). Following 4 mm of bone loss, stress levels increased and localized in the cervical third (yellow–green areas) of the residual socket. Across all three load magnitudes and for both failure models, the quantitative findings remained consistent.

This research involved a numerical analysis comprising 405 finite element simulations across 81 three-dimensional models, designed to evaluate the biomechanical response of trabecular bone subjected to progressive horizontal periodontal loss under five orthodontic movements and three load levels. It represents the first investigation of its kind, as no previous FEA-based studies have specifically analyzed the trabecular component in such conditions. Furthermore, existing data on safe orthodontic force limits for compromised periodontium are lacking, except for those provided by our own previous work [1, 2, 17, 20, 22, 23]. Prior reports (still debated) suggested that up to 1.5 N may be safe for intact tissues [16, 24, 30].

The scientific relevance of our results lies in demonstrating that finite element analyses can yield biomechanically valid outputs consistent with clinical phenomena. Unlike earlier numerical publications [4–15], only our prior studies [1, 2, 17, 20, 22] have verified their clinical applicability or fully adhered to standard FEA protocols [4-6, 11, 21]. Clinically, this work contributes a comprehensive biomechanical depiction of orthodontic movement in progressive periodontal degradation under variable loading—marking the first systematic assessment of this essential issue.

To ensure validity, our FEA approach strictly complied with established numerical modeling principles—including the selection of failure criteria appropriate for material type, boundary condition definitions, and anatomically accurate 3D modeling [1, 2, 17, 19–22]. The employed stress criteria, which characterize ductile material mechanics similar to dental structures [1, 2, 17], were Von Mises (overall homogeneous stress) and Tresca (shear, non-homogeneous stress). Their discrepancy, typically between 1.15–1.30, was confirmed here at an average of 1.09–1.21, aligning well with literature data. Boundary conditions were modeled assuming isotropy, linear elasticity, and either homogeneity or non-homogeneity, consistent with previously established FEA frameworks [4–15]. These were correlated with physiological MHP values (16–22

kPa) and recognized clinical biomechanical norms [1, 2, 17, 19, 20, 22].

Because both criteria yielded comparable color distributions, the difference between assuming homogeneous (VM) and non-homogeneous (T) trabecular structures appears minimal. Each successfully represented realistic biomechanical responses, in agreement with clinical and prior experimental data [1, 17]. Additionally, these modeling assumptions held true for loads up to 2.4 N, confirming their appropriateness for trabecular bone evaluation. A strong overlap between total and shear stress was noted, both visually and numerically, across all movements, bone-loss stages, and load intensities—Tresca stresses averaging 1.09–1.21× higher than Von Mises, a difference critical for assessing ischemic and resorptive risk where MHP thresholds are surpassed.

All stress distribution projections **(Figures 3–7)** demonstrated color-coded patterns that accurately reflected orthodontic tooth movement mechanics, consistent with established clinical findings. Among the analyzed movements, rotation generated the greatest stress, followed closely by translation, particularly in cases with a compromised periodontium, where ischemic and resorptive risks intensified as bone loss advanced. In contrast, intrusion and extrusion presented the lowest stress levels, supporting previous research [1, 2, 17].

For a healthy periodontium, forces up to 1.2 N appear to pose minimal ischemic or resorptive risk. However, in a reduced periodontium, a 1.2 N load is advisable only for intrusion and extrusion, and with caution when bone loss exceeds 7 mm. For rotation, translation, and tipping, forces beyond 0.6 N increase ischemic and resorptive likelihoods; hence, load reduction is recommended—consistent with prior guidelines suggesting 0.2–0.4 N to minimize risks [1, 17], and with Proffit *et al*. [30], who recommended 0.1–1 N. The periodontal ligament (PDL) and neurovascular bundle (NVB) represent the most vulnerable components within the periodontium, as they are highly responsive to orthodontic loading, serving mainly in force absorption and dissipation [1, 17]. Conversely, trabecular bone exhibits greater resistance. Therefore, in reduced periodontal conditions, orthodontic forces should primarily account for the sensitivity of the PDL–NVB complex rather than the bone matrix [1, 3, 17, 18, 23, 25, 26].

In clinical biomechanics, pure tooth movements seldom occur—unlike the isolated simulations used in this analysis—resulting in a composite stress distribution pattern in reality, typically with lower magnitudes than those modeled. In both intact and reduced periodontal structures, a 2.4 N load must be applied with caution, as it surpasses the maximum hydrostatic pressure (MHP) threshold considerably (up to 29× in 8 mm bone loss during rotation), greatly heightening ischemic and resorptive potential [1, 17].

Beyond ischemic and resorptive complications, orthodontic root resorption—both internal and external—is a frequent consequence of surpassing the MHP, often accompanied by further periodontal deterioration [2, 31–41]. Although the precise mechanobiological processes remain partially unresolved [42–46], evidence indicates that for intact periodontium, safe force levels range between 0.5–1 N, with an expanded range of 0.28–3.31 N also reported [19, 24, 47–51]. Nonetheless, root resorption can result from multiple interacting factors beyond orthodontic forces alone [31, 32, 40, 49, 52–59].

Given that this study centers on the biomechanical response of orthodontic forces in intact versus reduced periodontium, the discussion focuses on orthodontically induced resorption under ischemic stress. Most investigations address root resorption only in intact periodontal tissues and within the aforementioned force ranges, while studies exploring resorption in reduced periodontium remain absent except for our prior analyses [2, 41]. Those finite element analysis (FEA) works, employing identical methodology and forces of 0.6 N and 1.2 N, indicated that rotation and translation entail higher external resorption risk once bone loss exceeds 4 mm, with risk severity rising alongside further degradation if applied force remains constant [2, 41]. Internal resorption was less pronounced but similarly progressive beyond 4 mm loss [2, 41]. High-stress zones on both internal and external surfaces were closely related, with rotation and tipping posing the highest pulp chamber resorption risk, which declined with increasing bone loss [2, 41]. Both numerical analyses concluded that maintaining the same orthodontic force as periodontal breakdown advances leads to a proportional escalation in resorptive risk [2, 41], findings that align with the present study's results.

Biomechanically, in an intact periodontium, the PDL–NVB complex maintains its full absorptive and dissipative capacity, allowing stress to distribute evenly throughout the alveolar socket and the surrounding trabecular bone network. In contrast, a reduced periodontium shows clear stress accumulation, particularly within the cervical third of the remaining alveolar socket once 4 mm of bone loss occurs, across all orthodontic force directions and magnitudes. This redistribution arises from the diminished surface area of the periodontal ligament, altering the stress

transmission pattern. Consequently, a 4 mm loss appears to represent a threshold point signaling a distinct shift in stress distribution during progressive periodontal degradation, consistent with prior investigations [1, 17]. Overall, a marked association was observed between the degree of bone loss, altered stress localization (especially around the alveolar crest after 4 mm), and increased stress magnitudes (often surpassing the MHP), corroborating previous findings [1, 17, 23].

Numerous finite element analyses (FEA) have been conducted on intact bone–implant systems [4–12], where the cortical layer surrounding the implant was evaluated using comparable failure criteria (Von Mises), boundary conditions (isotropy, homogeneity, and linear elasticity), and sample size (a single model or patient with limited simulations). These works generally identified qualitative stress accumulation near the cervical third of the implant socket. However, since PDL–NVB structures were excluded, direct comparison or extended correlation with the present findings remains unattainable.

Only three numerical models involving tooth–bone systems in an intact periodontium have been published [13–15], and none investigated reduced periodontium conditions. These studies adopted similar boundary and failure assumptions as ours, each based on one specimen.

Shaw *et al*. [13] (one upper incisor model; intact periodontium; 11,924 elements; 20,852 nodes; Von Mises and maximum principal stress criteria; unspecified load) reported relatively low cervical stress levels — 1.664 KPa for intrusion/extrusion, 0.6 KPa for translation, 0.54 KPa for tipping, and 0.015 KPa for rotation — under similar movement categories. Variations are attributed to different force magnitudes, distinct tooth morphologies (incisor versus premolar in our model), and lower anatomical precision (507 fewer elements compared with our dataset).

Field *et al*. [14] conducted a numerical simulation (n = 1) assessing tipping under 0.35 N applied and 0.5 N resultant load across two mandibular 3D intact periodontium models — one multi-tooth model (32,812 elements; incisor, canine, premolar) and one single-tooth model (23,565 elements; canine). Using Von Mises, maximum/minimum principal stress, and hydrostatic pressure criteria, they observed higher stress in the multi-tooth setup. Although their stress distribution zones resembled ours (notably near the alveolar socket), the reported magnitudes were unrealistically elevated (red intensity for only 0.35 N), which conflicts with clinical biomechanics. If accurate, such stress levels would predict severe ischemia and resorption for 0.35 N, which does not occur clinically. Their trabecular stress values reached 34.2 KPa (single-tooth) and 125.6 KPa (multi-tooth, 4× higher), while ours were 14.54 KPa for 0.6 N, more in line with physiological reality. Additionally, their PDL stresses (235.5–324.5 KPa) exceeded normal MHP values (16–22 KPa) by roughly 15×, suggesting ischemic damage even in healthy models [30]. Such disparities likely stem from coarse mesh resolution (23,565–32,812 elements; 1.2 mm global size) compared to our high-resolution mesh (5.06–6.05 million elements; 0.08–0.116 mm), along with boundary condition inaccuracies and poor alignment with clinical evidence.

Merdji *et al*. [15] analyzed three forces (10 N intrusion; 3 N tipping and translation) using FEA (Von Mises) on a single lower third molar with an intact periodontium (142,305 elements; element size 0.25–1 mm). They reported stress clustering near the cervical third, resembling our pattern. However, modeling and anatomical simplifications produced inflated stress magnitudes — 10.5 MPa (intrusion), 11.5 MPa (tipping), and 16.83 MPa (translation) — compared to our results (40.7 KPa, 58.17 KPa, and 79.25 KPa at 2.4 N), emphasizing substantial quantitative deviation.

The limitations of FEA lie in its incomplete ability to replicate clinical dynamics. Advanced algorithms must be developed to realistically reproduce tooth motion, tissue interactions, and micro-architectural responses. Given that dental FEA modeling remains an emerging field—with few studies offering validated corrections for its current constraints—our work builds upon available evidence to address several methodological challenges [4-6, 11, 21].

Our earlier investigations demonstrated that dental tissues behave as ductile-like materials exhibiting partial brittle flow, making ductile failure criteria—notably Tresca (T) and Von Mises (VM)—the most accurate predictors, with T being the more reliable [1, 2, 17, 20, 22, 23]. Additionally, within the 0–2.4 N force range, our boundary conditions (isotropy, linear elasticity, and material homogeneity/non-homogeneity) remain valid [1, 17, 20]. These same simplifications have been routinely applied in prior dental FEA literature [4–15, 21], despite the known anatomical reality of anisotropy, non-homogeneity, and nonlinear elasticity [1, 2, 17, 22].

In this research, the non-homogeneous properties of the modeled materials were handled through the use of the Tresca failure criterion, which is specifically formulated for analyzing non-homogeneous materials. The assumption of linear elasticity is valid only under

minor load conditions, where both displacement and deformation remain minimal [1, 2, 17].

The question of anisotropy versus isotropy continues to be debated, as available studies present conflicting results, focusing primarily on the periodontal ligament (PDL) [27-29]. Hemanth *et al*. [27, 28] reported nonlinear numerical outcomes that were 20–50% lower than those obtained under linear conditions (within the 0.3–1 N range for intrusion and tipping). However, these studies classified the PDL of the upper incisor as a brittle-type material, analyzed under the maximum principal stress criterion, despite its clinically recognized ductile-like nature. This choice substantially altered the biomechanical interpretation. Furthermore, their applied forces were below 1 N, a range where, according to classical mechanics, all materials display linear elastic behavior. Conversely, Toms *et al*. [29] found higher stress values in the PDL of the lower premolar (under 1 N extrusion) for the nonlinear model compared with the linear one. Yet, despite adopting the Von Mises criterion, their simulated stress distribution patterns were unrealistic and inconsistent with accepted clinical data.

Within our boundary condition framework, a uniformly loaded area was applied through a linear ramp function, gradually increasing to the full load to avoid premature failure, localized stress accumulation, and computational errors. The reviewed FEA studies did not specify comparable loading conditions; hence, part of the observed variability between their findings and ours may stem from differences in the loading phase.

The sample size in FEA research is commonly limited to a single model [4–16, 21, 24, 27–29], since these analyses are descriptive simulations rather than clinical experiments [1, 17, 22]. Each FEA study can yield different outcomes by altering only a few input parameters, even when based on a single digital model. Nevertheless, a larger dataset enhances precision and reliability. For this reason, our investigation employed nine samples—representing nine patients, 81 three-dimensional models, and 405 total simulations.

Despite inherent constraints, finite element analysis remains the only tool capable of examining individual dental tissue components in isolation and providing insights that are applicable to both clinical and research settings. This work aimed to analyze the biomechanical response of periodontal tissues experiencing varying degrees of bone loss (0–8 mm) under different orthodontic forces and movement types, while also evaluating the tissue-level ischemic and resorptive risks that arise during orthodontic intervention. To achieve anatomical precision, our 3D digital models were reconstructed from CBCT radiographs, faithfully replicating the natural geometric morphology of periodontal structures. Since living periodontal tissues are anisotropic, non-homogeneous, and nonlinear in elasticity, it was essential that the chosen failure criterion align with these physical traits. The Tresca model best satisfied these requirements; however, its validity still necessitates comparison with clinical and experimental data for verification.

Conclusion

1. Both failure models produced comparable qualitative outputs, while quantitatively, Tresca (T) yielded results 1.09–1.21 times higher than Von Mises (VM). No noticeable qualitative difference appeared among the three orthodontic loads. Quantitatively, stresses approximately doubled at 1.2 N and quadrupled at 2.4 N, relative to 0.6 N.
2. Rotational and translational movements, followed by tipping, generated the highest biomechanical stresses, particularly in the reduced periodontium, thereby heightening ischemic and resorptive susceptibility.
3. In an intact periodontium, forces up to 1.2 N presented no major ischemic or resorptive threats. Conversely, in a reduced periodontium, 1.2 N should be limited to extrusion and intrusion, while loads exceeding 0.6 N substantially increase risk levels for other movements.
4. Under biomechanical evaluation, an intact periodontium displayed widespread stress distribution across the alveolar socket and trabecular bone, whereas a reduced periodontium revealed localized stress buildup around the cervical third of the residual alveolar socket once 4 mm of bone loss occurred.
5. The 4 mm threshold appears to serve as a biomechanical indicator for stress redistribution during periodontal degradation, showing a strong correlation between bone loss, stress concentration near the alveolar socket, and increased stress magnitude.

Practical implications

Clinically, patients often present with varying stages of periodontal breakdown; thus, understanding how bone loss alters stress behavior is essential. The safe force range remains debated even for an intact periodontium, and data for compromised tissues are limited. Recognizing that forces ≤1.2 N are generally safe for healthy tissues and that >0.6 N should be applied cautiously in reduced conditions is critical to

minimizing ischemic and resorptive events. Moreover, knowing that stress disperses widely in intact tissues but concentrates near the alveolar crest once 4 mm of loss is reached provides valuable clinical insight. This study extends current understanding of trabecular bone biomechanics under progressive periodontal deterioration.

From a research perspective, given the scarcity of data addressing trabecular bone behavior, this study contributes a detailed and realistic overview of the biomechanical responses of both intact and reduced periodontium under varying orthodontic forces and motion types. It is uncommon for FEA investigations to produce results that align so closely with clinical observations and physiological constants. The present findings also assist researchers in refining their understanding of failure criteria, boundary condition design, and FEA methodology, advancing the production of accurate, clinically relevant dental simulations within the engineering domain.

Acknowledgments: None

Conflict of Interest: None

Financial Support: None

Ethics Statement: None

References

1. Moga RA, Olteanu CD, Buru SM, Botez MD, Delean AG. Cortical and trabecular bone stress assessment during periodontal breakdown—A comparative finite element analysis of multiple failure criteria. Medicina. 2023;59(8):1462.
2. Moga RA, Olteanu CD, Botez MD, Buru SM. Assessment of the orthodontic external resorption in periodontal breakdown—A finite elements analysis (Part I). Healthcare. 2023;11(11):1447.
3. Wang L, You X, Zhang L, Zhang C, Zou W. Mechanical regulation of bone remodeling. Bone Res. 2022;10(1):16.
4. Prados-Privado M, Martínez-Martínez C, Gehrke SA, Prados-Frutos JC. Influence of bone definition and finite element parameters in bone and dental implants stress: A literature review. Biology (Basel). 2020;9(8):224.
5. Yamanishi Y, Yamaguchi S, Imazato S, Nakano T, Yatani H. Effects of the implant design on peri-implant bone stress and abutment micromovement: Three-dimensional finite element analysis of original computer-aided design models. J Periodontol. 2014;85(3):e333–8.
6. Pérez-Pevida E, Brizuela-Velasco A, Chávarri-Prado D, Jiménez-Garrudo A, Sánchez-Lasheras F, Solaberrieta-Méndez E, et al. Biomechanical consequences of the elastic properties of dental implant alloys on the supporting bone: Finite element analysis. Biomed Res Int. 2016;2016(1):1850401.
7. Shash YH, El-Wakad MT, Eldosoky MAA, Dohiem MM. Evaluation of stress and strain on mandible caused using "All-on-Four" system from PEEK in hybrid prosthesis: Finite-element analysis. Odontology. 2022;111(4):618–29.
8. Park JM, Kim HJ, Park EJ, Kim MR, Kim SJ. Three-dimensional finite element analysis of the stress distribution around the mandibular posterior implant during non-working movement according to the amount of cantilever. J Adv Prosthodont. 2014;6(5):361–71.
9. Cicciù M, Cervino G, Milone D, Risitano G. FEM investigation of the stress distribution over mandibular bone due to screwed overdenture positioned on dental implants. Materials (Basel). 2018;11(9):1512.
10. Tawara D, Nagura K. Predicting changes in mechanical properties of trabecular bone by adaptive remodeling. Comput Methods Biomech Biomed Engin. 2017;20(4):415–25.
11. Aunmeungtong W, Khongkhunthian P, Rungsiyakull P. Stress and strain distribution in three different mini dental implant designs using implant retained overdenture: A finite element analysis study. Oral Implantol (Rome). 2016;9(4):202–12.
12. Merdji A, Bachir Bouiadjra B, Achour T, Serier B, Ould Chikh B, Feng ZO. Stress analysis in dental prosthesis. Comput Mater Sci. 2010;49(1):126–33.
13. Shaw AM, Sameshima GT, Vu HV. Mechanical stress generated by orthodontic forces on apical root cementum: A finite element model. Orthod Craniofac Res. 2004;7(2):98–107.
14. Field C, Ichim I, Swain MV, Chan E, Darendeliler MA, Li W, Li Q. Mechanical responses to orthodontic loading: A 3-dimensional finite element multi-tooth model. Am J Orthod Dentofacial Orthop. 2009;135(2):174–81.
15. Merdji A, Mootanah R, Bachir Bouiadjra BA, Benaissa A, Aminallah L, Ould Chikh El B, Mukdadi S. Stress analysis in single molar tooth. Mater Sci Eng C Mater Biol Appl. 2013;33(2):691–8.
16. Shetty B, Fazal I, Khan SF. FEA analysis of normofunctional forces on periodontal elements in

different angulations. Bioinformation. 2022;18(4):245–50.
17. Moga RA, Olteanu CD, Delean AG. Investigating the ability of the tooth and surrounding support tissues to absorb and dissipate orthodontic loads during periodontal breakdown—Finite elements analysis. Appl Sci (Basel). 2024;14(3):1041.
18. Wu V, Schulten E, Helder MN, Ten Bruggenkate CM, Bravenboer N, Klein-Nulend J. Bone vitality and vascularization of mandibular and maxillary bone grafts in maxillary sinus floor elevation: A retrospective cohort study. Clin Implant Dent Relat Res. 2023;25(2):141–51.
19. Wu J, Liu Y, Wang D, Zhang J, Dong X, Jiang X, Xu X. Investigation of effective intrusion and extrusion force for maxillary canine using finite element analysis. Comput Methods Biomech Biomed Engin. 2019;22(11):1294–302.
20. Moga RA, Buru SM, Olteanu CD. Assessment of the best FEA failure criteria (Part I): Investigation of the biomechanical behavior of PDL in intact and reduced periodontium. Int J Environ Res Public Health. 2022;19(19):12424.
21. Perez-Gonzalez A, Iserte-Vilar JL, Gonzalez-Lluch C. Interpreting finite element results for brittle materials in endodontic restorations. Biomed Eng Online. 2011;10(1):44.
22. Moga RA, Olteanu CD, Botez M, Buru SM. Assessment of the maximum amount of orthodontic force for dental pulp and apical neuro-vascular bundle in intact and reduced periodontium on bicuspids (Part II). Int J Environ Res Public Health. 2023;20(2):1179.
23. Moga RA, Buru SM, Chiorean CG. Overall stress in periodontal ligament under orthodontic movement during a periodontal breakdown. Am J Orthod Dentofacial Orthop. 2022;161(2):e127–e135.
24. Wu J, Liu Y, Li B, Wang D, Dong X, Sun Q, et al. Numerical simulation of optimal range of rotational moment for the mandibular lateral incisor, canine and first premolar based on biomechanical responses of periodontal ligaments: A case study. Clin Oral Investig. 2021;25(4):1569–77.
25. Burr DB. Why bones bend but don't break. J Musculoskelet Neuronal Interact. 2011;11(4):270–85.
26. Hart NH, Nimphius S, Rantalainen T, Ireland A, Siafarikas A, Newton RU. Mechanical basis of bone strength: Influence of bone material, bone structure and muscle action. J Musculoskelet Neuronal Interact. 2017;17(3):114–39.
27. Hemanth M, Deoli S, Raghuveer HP, Rani MS, Hegde C, Vedavathi B. Stress induced in the periodontal ligament under orthodontic loading (Part I): A finite element method study using linear analysis. J Int Oral Health. 2015;7(9):129–33.
28. Hemanth M, Deoli S, Raghuveer HP, Rani MS, Hegde C, Vedavathi B. Stress induced in periodontal ligament under orthodontic loading (Part II): A comparison of linear versus non-linear FEM study. J Int Oral Health. 2015;7(9):114–8.
29. Toms SR, Eberhardt AW. A nonlinear finite element analysis of the periodontal ligament under orthodontic tooth loading. Am J Orthod Dentofacial Orthop. 2003;123(6):657–665.
30. Proffit WR, Fields HW, Sarver DM, Ackerman JL. Contemporary Orthodontics. 5th ed. St. Louis (MO): Elsevier; 2012.
31. Villaman-Santacruz H, Torres-Rosas R, Acevedo-Mascarúa AE, Argueta-Figueroa L. Root resorption factors associated with orthodontic treatment with fixed appliances: A systematic review and meta-analysis. Dent Med Probl. 2022;59(4):437–50.
32. Laskowska J, Paradowska-Stolarz A, Miralles-Jordá L, Schutty D, Mikulewicz M. Complication of orthodontic treatment: A case report on severe apical root resorption (ARR) in a patient with Turner syndrome. Children (Basel). 2024;11(3):358.
33. Zhang X, Zhou H, Liao X, Liu Y. The influence of bracket torque on external apical root resorption in bimaxillary protrusion patients: A retrospective study. BMC Oral Health. 2022;22(1):7.
34. Cheng LL, Turk T, Elekdag-Turk S, Jones AS, Petocz P, Darendeliler MA. Physical properties of root cementum. Part 13: Repair of root resorption 4 and 8 weeks after the application of continuous light and heavy forces for 4 weeks: A microcomputed-tomography study. Am J Orthod Dentofacial Orthop. 2009;136(3):320.e1–320.e10.
35. Zhong J, Chen J, Weinkamer R, Darendeliler MA, Swain MV, Sue A, et al. In vivo effects of different orthodontic loading on root resorption and correlation with mechanobiological stimulus in periodontal ligament. J R Soc Interface. 2019;16(153):20190108.
36. Zhang X, Li MQ, Guo J, Yang HW, Yu J, Li GJ. An analysis of the optimal intrusion force of the maxillary central incisor with root horizontal resorption using the finite element method and curve fitting. Comput Methods Biomech Biomed Engin. 2022;25(13):1471–86.

37. Patel S, Saberi N, Pimental T, Teng PH. Present status and future directions: Root resorption. Int Endod J. 2022;55(Suppl 4):892–921.
38. Deng Y, Sun Y, Xu T. Evaluation of root resorption after comprehensive orthodontic treatment using cone beam computed tomography (CBCT): A meta-analysis. BMC Oral Health. 2018;18(1):116.
39. Chan E, Darendeliler MA. Physical properties of root cementum. Part 5: Volumetric analysis of root resorption craters after application of light and heavy orthodontic forces. Am J Orthod Dentofacial Orthop. 2005;127(2):186–95.
40. Lee YJ, Lee TY. External root resorption during orthodontic treatment in root-filled teeth and contralateral teeth with vital pulp: A clinical study of contributing factors. Am J Orthod Dentofacial Orthop. 2016;149(1):84–91.
41. Moga RA, Delean AG, Buru SM, Botez MD, Olteanu CD. Orthodontic internal resorption assessment in periodontal breakdown—A finite elements analysis (Part II). Healthcare (Basel). 2023;11(20):2622.
42. Rey D, Smit RM, Gamboa L. Orthodontic treatment in a patient with idiopathic root resorption: A case report. Dent Press J Orthod. 2015;20(4):108–117.
43. Iglesias-Linares A, Yañez-Vico RM, Ballesta S, Ortiz-Ariza E, Mendoza-Mendoza A, Perea E, et al. Interleukin 1 gene cluster SNPs (rs1800587, rs1143634) influence post-orthodontic root resorption in endodontic and their contralateral vital control teeth differently. Int Endod J. 2012;45(11):1018–26.
44. Iglesias-Linares A, Yañez-Vico RM, Ortiz-Ariza E, Ballesta S, Mendoza-Mendoza A, Perea E, Solano-Reina E. Postorthodontic external root resorption in root-filled teeth is influenced by interleukin-1β polymorphism. J Endod. 2012;38(3):283–7.
45. Iglesias-Linares A, Yañez-Vico RM, Ballesta-Mudarra S, Ortiz-Ariza E, Mendoza-Mendoza A, Perea-Pérez E, et al. Interleukin 1 receptor antagonist (IL1RN) genetic variations condition post-orthodontic external root resorption in endodontically-treated teeth. Histol Histopathol. 2013;28(6):767–73.
46. Iglesias-Linares A, Yañez-Vico R, Ballesta-Mudarra S, Ortiz-Ariza E, Ortega-Rivera H, Mendoza-Mendoza A, et al. Postorthodontic external root resorption is associated with IL1 receptor antagonist gene variations. Oral Dis. 2012;18(2):198–205.
47. Pereira SA, Melo A, Resende E, Regateiro F, Coimbra Silva H. Antagonistic effect of IL1 variants in periodontitis and external apical root resorption: Evidence from a literature review. Arch Oral Biol. 2018;95(1):195–201.
48. Wu JL, Liu YF, Peng W, Dong HY, Zhang JX. A biomechanical case study on the optimal orthodontic force on the maxillary canine tooth based on finite element analysis. J Zhejiang Univ Sci B. 2018;19(7):535–546.
49. Alhadainy HA, Flores-Mir C, Abdel-Karim AH, Crossman J, El-Bialy T. Orthodontic-induced external root resorption of endodontically treated teeth: A meta-analysis. J Endod. 2019;45(5):483–9.
50. Moga RA, Olteanu CD, Buru SM, Botez MD, Delean AG. Finite elements analysis of biomechanical behavior of the bracket in a gradual horizontal periodontal breakdown—A comparative analysis of multiple failure criteria. Appl Sci (Basel). 2023;13(15):9480.
51. Kochar GD, Jayan B, Chopra SS, Mechery R, Goel M, Verma M. Interdisciplinary management of patient with advanced periodontal disease. Int J Orthod (Milwaukee). 2016;27(1):51–6.
52. Sivakumar A, Raju MA, Sunny J, Cyriac R, Bhat S, Mohandas AA, Divya B. Collaborative management of a young patient with generalized aggressive periodontitis. Int J Orthod (Milwaukee). 2014;25(1):27–31.
53. Pamukçu H, Polat-Özsoy Ö, Gülşahi A, Özemre M. External apical root resorption after nonextraction orthodontic treatment with labial vs lingual fixed appliances. J Orofac Orthop. 2020;81(1):41–51.
54. Yi J, Li M, Li Y, Li X, Zhao Z. Root resorption during orthodontic treatment with self-ligating or conventional brackets: A systematic review and meta-analysis. BMC Oral Health. 2016;16(1):125.
55. Alves Otelakoski B, Magno Gonçalves F, Marques de Mattos de Araujo B, Zeigelboim BS, Veríssimo Meira Taveira K, Sampaio Santos R, et al. Comparison of orthodontic root resorption of root-filled and vital teeth: A meta-analysis. J Am Dent Assoc. 2022;153(6):532–541.e7.
56. Ioannidou-Marathiotou I, Zafeiriadis AA, Papadopoulos MA. Root resorption of endodontically treated teeth following orthodontic treatment: A meta-analysis. Clin Oral Investig. 2013;17(7):1733–44.
57. Zhao D, Xue K, Meng J, Hu M, Bi F, Tan X. Orthodontically induced external apical root resorption considerations of root-filled teeth vs

vital pulp teeth: A systematic review and meta-analysis. BMC Oral Health. 2023;23(1):241.

58. Gravholt CH, Viuff MH, Brun S, Stochholm K, Andersen NH. Turner syndrome: Mechanisms and management. Nat Rev Endocrinol. 2019;15(10):601–14.
59. Leone PE, Yumiceba V, Jijón-Vergara A, Pérez-Villa A, Armendáriz-Castillo I, García-Cárdenas JM, et al. Cytogenetic and genomic analysis of a patient with Turner syndrome and t(2;12): A case report. Mol Cytogenet. 2020;13(1):46.